Calibration and performance of the ISO Long-Wavelength Spectrometer

Astron. Astrophys. 315, L43–L48 (1996)

ASTRONOMY AND ASTROPHYSICS

Calibration and performance of the ISO Long-Wavelength Spectrometer

B.M. Swinyard[1], P.E. Clegg[2], P.A.R. Ade[2], C. Armand[3], J.-P. Baluteau[4], M.J. Barlow[5], J.-C. Berges[6], M. Burgdorf[3], E. Caux[7], C. Ceccarelli[8], R. Cerulli[8], S.E. Church[9], S. Colgan[10], F. Cotin[7], P. Cox[11], P. Cruvellier[6], G.R. Davis[12], A. DiGiorgio[3], R.J. Emery[1], D. Ewart[3], J. Fischer[13], I. Furniss[5], W.M. Glencrossi[5], M. Greenhouse[14], M.J. Griffin[2], C. Gry[3,6] M.R. Haas[10], M. Joubert[15], K.J. King[1], T. Lim[3], R. Liseau[16], S. Lord[17], D. Lorenzetti[18], S. Molinari[3], D.A. Naylor[19], B. Nisini[8], A. Omont[20], R. Orfei[8], T. Patrick[21], D. Pequignot[22], D. Pouliquen[6], M.C. Price[3], Nguyen-Q-Rieu[23], F.D. Robinson[24], M. Saisse[6], P. Saraceno[8], G. Serra[7], S.D. Sidher[3], H.A. Smith[14], L. Spinoglio[8], D. Texier[3], W.A. Towlson[5], N. Trams[3], S.J. Unger[1], and G.J. White[2]

[1] Rutherford Appleton Laboratory, Chilton, Didcot, Oxon OX11 0QX, UK
[2] Queen Mary and Westfield College, University of London, Mile End Road, London E1 4NS, UK
[3] The LWS Instrument-Dedicated Team, ISO Science Operations Centre, Villafranca, Spain
[4] Observatoire de Marseille, 2 place de Verrier, F-13248 Marseille, France
[5] Dept. of Physics and Astronomy, University College London, Gower Street, London WC1E 6BT, UK
[6] Laboratoire d'Astronomie Spatiale, BP 8, Les Trois Lucs, F-13376 Marseille, France
[7] Centre d'Etude Spatiale des Rayonnements, 9, avenue de Colonel Roche, F-31029 Toulouse, France
[8] CNR-Istituto de Fisica dello Spazio Interplanetario, CP 27, I-00044 Frascati, Italy
[9] Observational Cosmology, MC 59-33, California Institute of Technology, Pasadena, CA 91125, USA
[10] Nasa Ames Reaserch Center, ms 245-6 Astrophysics Branch, Space Science Division, Moffet Field, CA 94035 1000, USA
[11] Universitie de Paris XI, Batiment 121, F-91405 Orsay, France
[12] Institute of Space and Atmospheric Studies, University of Saskatchewan, 116 Science Place, Saskatoon, Saskatchewan, S7N 5E2, Canada
[13] Naval Research Laboratory, Remote Sensing Division, 4555 Overlook Avenue SW, Washington DC 20375, USA
[14] National Air and Space Museum, Smithsonian Institution, Laboratory for Astrophysics, Washington, DC 20560, USA
[15] CNES, 2 pace Maurice Quentin, F-75001 Paris, France
[16] Stockholm Observatory, S-13336, Saltsjobaden, Sweden
[17] IPAC/Caltech, ms 100-22, Pasadena, CA 91125, USA
[18] Osservatorio Astronomico di Roma, I-00040 Monte Porzio, Italy
[19] Department of Physics, University of Lethbridge, 4401 University Drive, Lethbridge, Alberta, T1K 3M4, Canada
[20] Institut d'Astrophysique, 98bis boulevard Arago, F-75014 Paris, France
[21] Mullard Space Science Laboratory, Holmbury St Mary, Dorking, Surrey, RH5 6NT, UK
[22] Observatoire de Paris, Section d'Astrophysique, F-92190 Paris, France
[23] Observatoire de Paris, 61 avenue de l'Observatoire, F-75014 Paris, France
[24] Code 717.3, NASA Goddard SFC, Greenbelt, MD 20771, USA

Received 5 August 1996 / Accepted 22 August 1996

Abstract. The wavelength and flux calibration, and the in-orbit performance of the Infrared Space Observatory Long-Wavelength Spectrometer (LWS) are described. The LWS calibration is mostly complete and the instrument's performance in orbit is largely as expected before launch. The effects of ionising radiation on the detectors, and the techniques used to minimise them are outlined. The overall sensitivity figures achieved in practice are summarised. The standard processing of LWS data is described.

Key words: artificial satellites – instrumentation: spectrographs – infrared: general

Send offprint requests to: B.M. Swinyard

1. Introduction

The Long Wavelength Spectrometer (LWS) is one of four instruments onboard the European Space Agency's Infrared Space Observatory, ISO (Kessler et al 1996). The instrument and its operation are described in more detail in Clegg et al. (1996) and Church et al. (1993). In this paper the in-orbit calibration

Table 1. Wavelength Accuracy of the LWS

Subsystem	$RMS Accuracy(\mu m)$
Grating	2.6×10^{-2}
FPS	8×10^{-4}
FPL	2.7×10^{-3}

scheme for the instrument is presented, together with a summary of the performance of the instrument as determined from calibration measurements.

The LWS uses a diffraction grating working in first and second order with a resolution element of 0.6 and 0.29 mm in first and second order respectively over a wavelength range from 43.0 to 196.9 mm. In addition there are two Fabry-Perot interferometers operated over the ranges 47-70 mm (FPS) and 70-196.6 mm (FPL) respectively, with a resolving power between 8100 and 8500 for FPS and 6800 and 9700 for FPL. The grating also performs the order sorting for the Fabry-Perots. The radiation dispersed from the grating is focused onto a linear detector array made up of one Ge:Be; five unstressed Ge:Ga and four stressed Ge:Ga photoconductive detectors with a concentric field of view on the sky. Bandpass filters located in front of the detectors define ten overlapping wavelength bands covering the wavelength range of the instrument. Each detector signal is read out by a JFET integrating amplifier which produces a voltage ramp the slope of which is proportional to the detector current. The current is measured by sampling this ramp at a frequency of 88 Hz.

The LWS observation parameters are controlled by means of Astronomical Observation Templates (AOTs). These are designed to maximise the efficiency of the instrument whilst giving the potential observer the minimum necessary interaction with the technical aspects of the instrument operation. At the time of writing, three of the four LWS AOTs have been commissioned and released for general use. The fourth (L03) is currently undergoing final in orbit testing.

2. Wavelength calibration and spectral resolution

Before the launch of ISO there was only a sparse knowledge of the lines available from astronomical sources that were likely to be suitable for the calibration of the LWS. End-to-end grating scans were therefore made to obtain spectral surveys of bright sources. More detailed grating scans were made on those sources which showed the strongest lines in order to achieve high signal to noise on the lines of interest. The lines finally used for grating wavelength calibration were OIII (51.814 μm); NIII (57.317 μm); OI (63.184 μm); OIII (88.356 μm); OI (145.525 μm); CII (157.741) and the CO J14-15 transition (173.631 μm). These lines give a comprehensive coverage across the LWS band with at least one line on each detector except LW2 and SW4. The NII(121.898 mm) line has subsequently been observed using LW2 confirming the wavelength calibration for this detector. The grating calibration obtained has been further refined using Fabry-Perot measurements of a bright continuum source (Jupiter) to give a series of accurate wavelength markers (Emery et al 1993).

Lines in the planetary nebulae NGC 6826 and NGC 7027, the bright HII region NGC 3603 and the reflection nebula NGC 7023 were also used to set up the mesh parallelism and to establish the wavelength calibration of the two Fabry-Perots. The wavelength calibration accuracy achieved for all three subsystems is given in Table 1. The long wavelength Fabry-Perot showed a problem with its operation that manifested itself as a loss of both transmission and resolution as the gap between the meshes was changed. This was traced to stray capacitance in the wiring harness causing an incorrect feed-back in the servo system that in turn led to a loss of parallelism. A solution to the problem has been implemented by updating the commanded offsets in the servo system about every 200 steps of the Fabry-Perot scan to maintain parallelism. This operation has been confirmed using both of the Fabry-Perot AOTs (L03 and L04). No line has yet been observed that is sufficiently narrow to allow the resolving power and transmission efficiency of the Fabry-Perots to be determined. However, none of the lines is resolved by the grating and the FWHM resolution has been confirmed as 0.29 mm for the second order and 0.6 mm for the first order.

3. Flux calibration and removal of instrument response

3.1. Primary flux standard

At present, the primary flux standard for the LWS is Uranus. Uranus has the advantages that it is bright (around 1 kJy at 100 μm), point-like in the LWS beam ($\sim$3 arcsec diameter), non-variable, and has a continuum spectrum which is featureless on the scale of the LWS spectral resolution. The model brightness temperature spectrum which we use for Uranus is based on measurements of the Voyager IRIS spectrometer which extend out to 50 μm wavelength (Hanel et al., 1986; B Conrath, private communication), and an extrapolation to longer wavelengths using an atmospheric model constrained to agree with ground-based submillimetre photometry (Griffin and Orton, 1993). The Uranian brightness temperature varies between 56 and 62 K over the LWS wavelength range. We estimate the absolute accuracy of the Uranus model to be within $\pm$5%. Observations of Mars later in the mission will be used to refine and cross check the absolute calibration scheme.

3.2. Removal of the instrument response function

The overall transmission function of the LWS is determined by the combination of the transmission of the optics and the Fabry-Perots, the bandpass filters, the efficiency of the grating and the optical chain (including diffraction effects from the ISO telescope), and the spectral response of the detectors. To remove the instrument response function from the astronomical spectra, a series of calibration tables (one for each detector) have been constructed. These tables were derived by dividing time-corrected and averaged sub-spectra of Uranus by the model

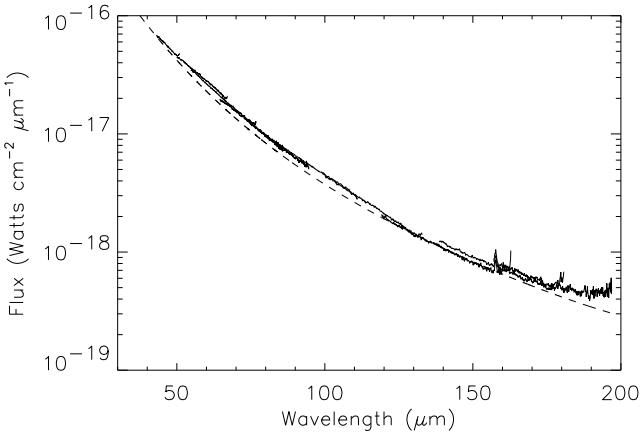

Fig. 1. LWS spectrum of the asteroid Ceres after correction using the illuminator flashes and the calibration against Uranus as described in the text. The dotted line is the flux predicted using the Standard Thermal Model (Lebofsky and Spencer 1989). The line at about 157 μm is due to CII emission from the cirrus.

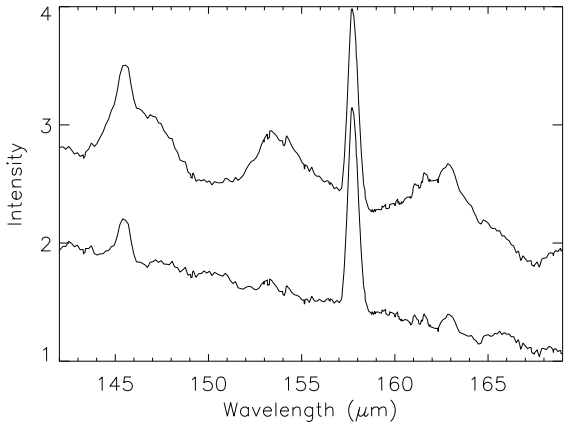

Fig. 2. The spectrum of DR21 West after flux calibration and removal of the instrument response (upper trace). The same spectrum is shown in the lower trace to show the effectiveness of the defringing algorithm. The spectrum has been arbitrarily displaced for clarity. The OI line at about 145μm the CII line at about 157μm and a CO line at about 163μm can be seen to be preserved whilst the fringing has been successfully removed from the continuum.

spectrum of Uranus described above. The tables contain the absolute responsivity (A W^{-1} cm^2.) of the LWS *referred to the entrance pupil of the ISO telescope*, within a spectral resolution element and within the beam of the LWS.

The signal to noise ratio per spectral element achieved in the measurement of the Uranus signal varies across the LWS wavelength range but is typically 350. All LWS grating spectra are divided by the spectrum of Uranus: the effective signal to noise on the calibrated continuum can therefore never be greater than this value, *no matter how high the signal to noise ratio achieved on the actual measurement.* Further measurements of the Uranus spectrum will be made in the near future to improve upon the signal to noise ratio.

Figure 1 shows the spectrum of the asteroid Ceres, calibrated using Uranus as described above and with the detector responsivity drift removed using the internal illuminators as described below. On the same plot is shown the predicted spectrum of Ceres for the date of observation calculated using the Standard Thermal Model (STM) of Lebofsky and Spencer (1989). It can be seen that the individual sub spectra of the detectors are matched to within 10% from one detector to another and the general shape of the STM is reproduced with the observed spectrum being generally higher than the predicted spectrum. This accuracy is not always achieved: variations between adjacent detectors as high as 30% are sometimes observed because the present scheme for correcting for the drift in responsivity of the detectors is not sufficiently accurate.

The matching of sub-spectra by use of the internal illuminators is one of the outstanding problems with the calibration of the LWS. Several methods of matching the sub-spectra have been tried. The overlap in the wavelength coverage of adjacent sub-spectra allows them to be scaled or shifted to match each other. Alternatively (Liu et al. 1996) a smooth function can be fitted to the continuum and the individual sub-spectra scaled to fit this function.

3.3. Defringing

Grating-mode spectra are often distorted by a large modulation (fringing), which is cosinusoidal in frequency space. A typical example, from a grating observation of DR21 West, is shown in the upper trace in Fig. 2. A systematic study of this phenomenon revealed that while point sources observed on-axis show negligible modulation, extended sources, and point sources observed off-axis, exhibit large modulation. Subsequent analysis has shown that this phenomenon could be caused by optical interference between multiply reflected beams in the LWS detector assembly. An extensive study of LWS spectra from a range of astronomical sources revealed that, whilst the amplitude of the interference component varied widely, the frequency and phase were stable for a given detector. We have constructed a defringing algorithm which makes use of this stability for use on all the detectors. The lower trace in fig. 2 (offset by 1 on the arbitrary intensity scale) shows the result of applying this algorithm to the spectrum of DR21 West in one of the LWS detector channels. It can be seen that, in this example, the large sinusoidal features in the continuum have been removed whilst preserving both weak and strong unresolved lines. Work is continuing to improve the defringing procedures.

3.4. The LWS beam

Analysis of the scans shows there to be a discrepancy between the beam width predicted from optical modelling of the ISO telescope and the LWS beam stop and that given by the measured profiles. At face value the data give a full width at half maximum of no more than 80 arcsecs, compared with a model value of 90 arcsecs at all wavelengths. The data also give some indication that the width may vary with wavelength with perhaps a smaller

width at longer wavelengths. At present this discrepancy is not understood and further modelling and observations are planned.

4. Ionising Radiation Effects

4.1. Detector curing

The dark current and responsivity of photoconductive detectors are influenced by ionising radiation. This was known before the launch of ISO and extensive tests were carried out using γ-ray sources to investigate these effects and to devise methods of "curing" the detectors in orbit (e.g., Price et al., 1992). When the satellite passes through the earth's radiation belts near perigee, the detectors are subjected to a high dose of ionising radiation, resulting in large increases in detector dark current, responsivity and noise. After perigee passage, the detectors are cured by increasing the bias voltage above the breakdown voltage for several minutes; this curing procedure has been found to work well in orbit.

Outside the radiation belts the hit-rate on the 1 mm^3 detectors from ionising cosmic rays is approximately one per detector per eight seconds. As the orbit progresses the accumulated dose leads to a steady increase in the responsivity of the detectors and some detectors exhibit excess noise and unstable behaviour after about 12 hours, unless they are recured. This second curing takes place during ground station hand-over near apogee and no observing time is lost.

4.2. Correction for dark current and responsivity variations

The evolution of the responsivity as a function of time around the orbit is monitored using the LWS internal illuminators. The change in responsivity is different for different detectors: the Ge:Be detector has roughly constant responsivity, but the variation is up to 80% for the stressed detectors. The curing procedure at the mid-point of the orbit returns the responsivity of all detectors to within 5% of that at the start of the orbit. Figure 3 shows the change in responsivity for one of the unstressed Ge:Ga detectors for a typical orbit. The slow, and essentially linear, upward drift of the responsivity can be seen together with the step downwards in responsivity following the mid-orbit curing procedure.

Astronomical signals must be corrected for the drift in responsivity and for detector dark current. For this reason each AOT includes a standard sequence of measurements of illuminator signals before and after the source is observed.

4.3. Effect of ionising radiation on sensitivity

When an ionising particle hits a detector a large amount of charge is deposited at the input of the integrating amplifier. This leads to a step discontinuity, or "glitch", in the amplifier output; these are removed from the data steam by processing software on the ground. The observed ionising hit rate is in broad agreement with the rate predicted before launch. However, the amount of charge generated within the detector is found to be much larger in many instances and the recovery from an individual hit takes longer than anticipated. In addition the detector output can become temporarily unstable following a hit. When operated at the optimum bias voltages and basic integration time (2 second) established in ground tests, it was found that these effects were such that the overall sensitivity and stability were degraded to such an extent as to make the detectors unusable. Experiments during checkout phase determined that the effects could be dramatically reduced by a combination of lower detector bias and shorter (0.5 second) basic integration time (ramp length). This results in a quicker recovery following a glitch, and in a stable baseline after the glitched data are removed. Reducing the detector bias and ramp length inevitably result in a loss of instantaneous sensitivity (Church et al. 1993) compared to that achieved on the ground. However, in the ionising radiation environment of ISO, it leads to a better overall performance because of the improvements in baseline stability and speed of recovery of the detectors.

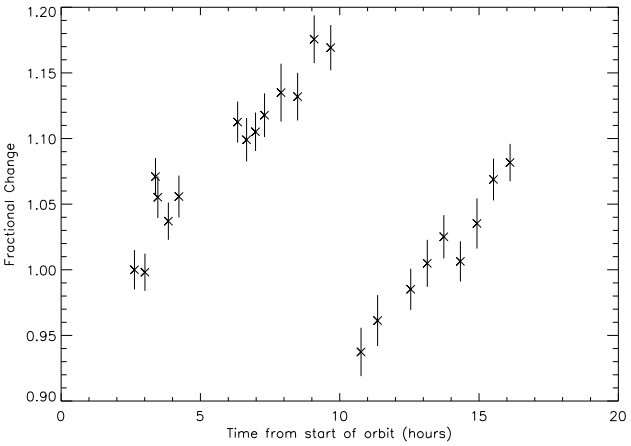

Fig. 3. Fractional change in responsivity vs. time in orbit for one of the unstressed Ge:Ga detectors as monitored by the internal illuminators. The sharp change in responsivity at the centre of the orbit is caused by the resetting of the detectors by the mid-orbit curing procedure.

Another consequence of ionising radiation in orbit is that it has been found that for most observations the optimum operating mode for the instrument is to work in the so called "fast-scanning" mode where a single ramp is taken per mechanism position and the integration time is built up using many scans of the mechanism.

5. Sensitivity achieved

The effects of ionising radiation and the measures needed to minimise them mean that the in-orbit NEPs of the detectors are increased by an average of a factor of 3.3 over the performance achieved in quiescent laboratory conditions: most of this increase arises from the need to use 0.5-second rather than 2-second integration ramps (Church et al 1993). Figure 4 shows the LWS sensitivity in grating mode as a function of wavelength together with the nominal wavelength coverage for each of the detector bands.

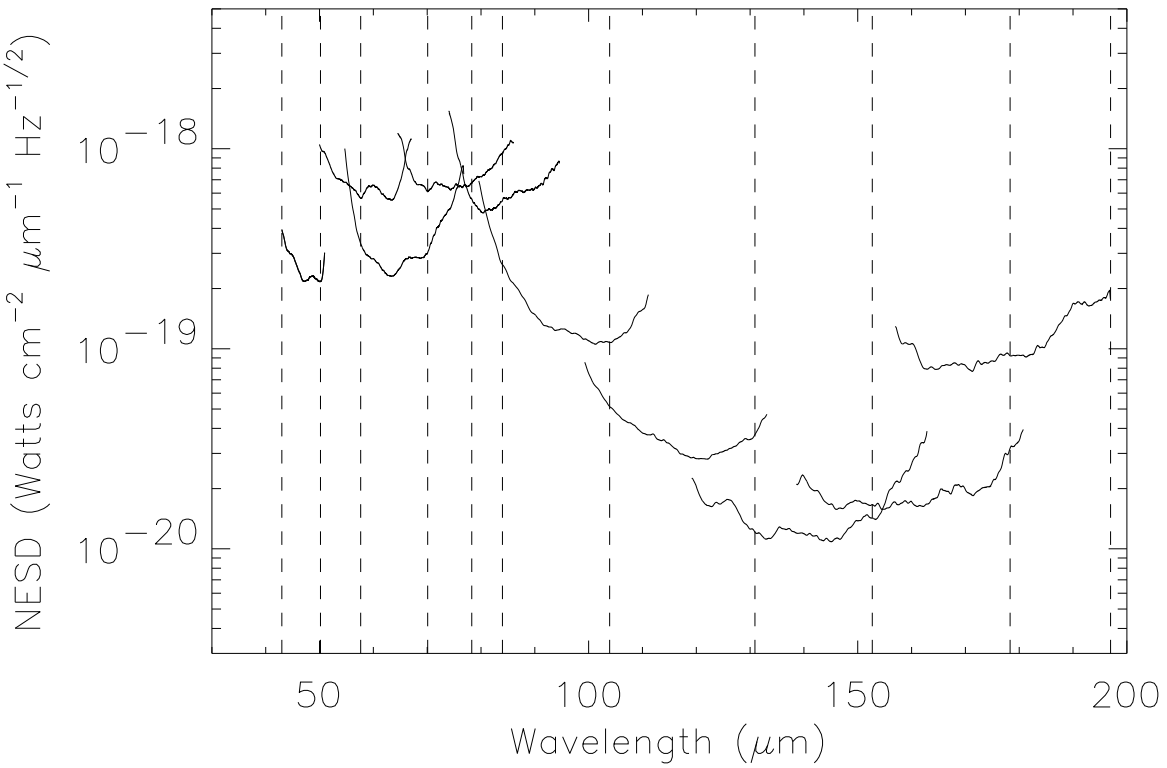

Fig. 4. Instrument sensitivity versus wavelength in grating mode. The vertical lines indicate the range of wavelength over which each detector is used in normal operation.

6. Pipeline processing of LWS data

The processing of the data from the LWS is split into two: the derivation of the Standard Processed Data (SPD) and Auto Analysis (AA). The SPD stage converts the detector data from raw engineering values into photocurrent by fitting a first or second order polynomial to individual ramps. The AA stage converts from photocurrent and mechanism position into flux and wavelength for both the grating and Fabry-Perot operating modes.

6.1. SPD Processing

The first portion of the data in the ramps are corrupted by the affects of electronic ringing in filters in the amplification chain and are not used for ramp fitting. The amount of data not used is fixed at 100 milliseconds for all cases except for three of the stressed Ge:Ga detectors (LW2, LW3 and LW4) where the first 150 milliseconds are not used for 0.5 second ramps. Before the ramp data have been fitted a glitch detection algorithm is applied that relies on the numerical differentiation of the ramp. If a glitch is detected then the rest of the data in the ramp following the glitch are discarded together with the subsequent two ramps. This has been found to be necessary as the responsivity of the detector has not recovered from the affects of the ionising radiation (see section 4) and the ramps are corrupted.

In general the response of the detector and integrating amplifier combination gives a curved ramp. In the present version of the pipeline software the linear term of a second order polynomial fit to the ramp is used to give a measure of the photocurrent. However, at low signal levels, the noise on the ramp is such as to make a second order polynomial fit inappropriate and a linear fit must be used. The SPD software changes from a first to second order fit at a given signal level. This is different for each detector and is calculated so as to effect as smooth a transition as possible from one to the other.

The illuminator flash data are also processed by the SPD stage and the average value of the photocurrent for each detector at each illuminator level is computed together with the average value of the background signal before and after the illuminators were operated. In the case of the opaque illuminator flashes (see Clegg et al 1996) this is a direct measurement of the dark current.

6.2. AA Processing

The AA stage first applies a wavelength scale: the grating position is converted to wavelength by reference to a table. For Fabry-Perot observations an algorithm converts the encoder position to physical gap and then to wavelength using the order of interference derived from the grating position.

For all observations the dark current is subtracted using the values calculated during the opaque illuminator flashes. Responsivity correction for grating scans is then made by dividing by the calibration tables described in section 3. The flux calibration is completed for grating scans by dividing by the appropriate

resolution element to give the final flux units of W cm^{-2} μm^{-1}. For Fabry-Perot data corrections are made for the underlying grating profile and transmission of the Fabry-Perots before applying the responsivity correction using the same tables as for the grating scans. The final spectrum is not divided by the resolution element of the Fabry-Perots and is therefore in units of W cm^{-2}.

The pipeline processing does not convert LWS flux densities to surface brightness because this requires knowledge of the source structure.

7. Conclusions and outstanding problems

The LWS calibration is mostly complete and the instrument's performance in orbit is largely as expected before launch. It is not yet clear why the LWS beam width is smaller than the expected 90 arcsec. A method has been devised to remove the fringes observed in LWS spectra and improved methods are being studied. Three of the four LWS AOTs have now been fully commissioned and are available for routine observations. The operating parameters and observing modes have been tailored to minimise the adverse effects of ionising radiation, at some inevitable cost to the instantaneous sensitivity. The LWS pipeline processing continues to evolve. The absolute flux calibration accuracy of the present pipeline analysis is better than 40substantially.

Acknowledgements. The Infrared Space Observatory is an ESA project funded by ESA member states (especially the PI countries: France, Germany, the Netherlands and the United Kingdom) and with the participation of ISAS and NASA.

References

Church, S.E., Griffin, M.J., Ade, P.A.R., Price, M.C.,Emery, R.J., Swinyard, 1993, B.M., Infrared Phys. 34, 389

Hanel, R.A., Conrath, B, Flasar, M, Kunde, V, Maguire, W, Pearl, J, Pirraglia, J, Samuelson, R, Cruikshank, D, Gautier, D, Gierasch, P, Horn, L, Schulte, P., 1986, Sci, 233, 70

Griffin, M.J. & Orton, G.S., 1993, Icarus 105, 537

Price, M.C., Griffin, M.J., Church, S.E., Murray, A.G., Ade, P.A.R. Proc. ESA Symposium on Photon Detectors for Space Instrumentation, Noordwijk, 10-12 Nov. 1992, ESA SP-356

Lui ,X-W., et al, 1996, this issue

Clegg, P.E., et al, 1996,this issue

Lebofsky, L., Spencer, J., 1989, in *Asteriods II*, R. Binzel ed, University of Arizona Press, Tucson.

Emery, R.J., King, K.J., Swinyard, B.M.,Church, S.E., 1993, *Infrared Detectors and Instrumentation*, SPIE 1946, 272.